WILEY-VCH

DOI: 10.1002/ ((please add manuscript number))
Article type: Full paper

Atomic layer engineering of epsilon-near-zero ultrathin films with controllable field enhancement

Sudip Gurung[1], Aleksei Anopchenko[1], Subhajit Bej[1], Jay Joyner[1], Jason D. Myers[2], Jesse Frantz[2], and Ho Wai Howard Lee[1,3*]

*Corresponding Author: E-mail: Howard_Lee@baylor.edu

[1] Department of Physics and Baylor Research and Innovation Collaborative (BRIC), Baylor University, Waco, TX 76798, United States
[2] Optical Sciences Division, U.S. Naval Research Laboratory, Washington, DC 20375, United States.
[3] The Institute for Quantum Science and Engineering, Texas A&M University, College Station, TX 77843, United States

Abstract

Enhanced and controlled light absorption as well as field confinement in an optically thin material are pivotal for energy-efficient optoelectronics and nonlinear optical devices. Highly doped transparent conducting oxide (TCO) thin films with near-zero permittivity can support ENZ modes in the so-called epsilon near zero (ENZ) frequency region, which can lead to perfect light absorption and ultra-strong electric field intensity enhancement (FIE) within the films. To achieve full control over absorption and FIE, one must be able to tune the ENZ material properties as well as the film thickness. Here, we experimentally demonstrate engineered absorption and FIE in aluminum doped zinc oxide (AZO) thin films via control of their ENZ wavelengths, optical losses, and film thicknesses, tuned by adjusting the atomic layer deposition (ALD) parameters such as dopant ratio, deposition temperature, and number of macro-cycles. We also demonstrate that under ENZ mode excitation, though the absorption and FIE are inherently related, the film thickness required for observing maximum absorption differs significantly from that for maximum FIE. This study on engineering ENZ material properties by optimizing the ALD process will be beneficial for the design and development of next-generation tunable photonic devices based on flat, zero-index optics.

Keywords: Thin film optics; Atomic layer deposition; Aluminum doped zinc oxide; Plasmonics; Epsilon-near-zero material; Epsilon-near-zero mode; Zero-index optics; Metamaterials; Perfect absorption; Electric field intensity enhancement.

1. Introduction

Over the last decade, there has been a resurgence of research interest in the optical properties of materials at their epsilon-near-zero (ENZ) frequencies [1], i.e. the frequencies at which real permittivity becomes zero (real part of complex permittivity $\varepsilon'=0$). Extensive study on light-matter interactions in the ENZ frequency regime has led to the discovery of a variety of novel phenomena [2] and has given birth to a new branch of photonics, zero-index photonics .

Furthermore, it has been demonstrated that ultra-thin ENZ films can support ENZ modes [3]. Excitation of such modes leads to the enhanced local density of optical states and, at certain conditions, to perfect absorption [4]. ENZ modes also ensure strong electric field confinement inside the films and have proven to be beneficial for enhancing light emission [5] and nonlinear optical responses [6].

For conventional metals and highly-doped semiconductors, the ENZ response occurs near their plasma frequencies [1b, 7]. Noble metals such as gold and silver exhibit ENZ points within the ultraviolet (UV) frequency range [8]. However, due to inter-band transitions, the optical losses (imaginary part of complex permittivity ε'') for metal in the UV region are too high to be useful for practical applications. Some other limitations include non-tunable optical properties due to high electron density, and incompatibility with standard nanofabrication processes. Hence, alternative plasmonic materials such as transparent conducting oxides which have significantly lower optical losses in combination with a large electrical conductivity have become more popular in recent years [7b, 7c]. Moreover, these materials are CMOS compatible and have been widely used in commercial devices such as displays, solar panels etc.

Highly-doped transparent conducting oxides (TCOs), which typically have carrier concentration in the range of 10^{19} cm^{-3} to 10^{21} cm^{-3}, exhibit ENZ points in the near-infrared frequency range. One of the most commonly used TCO material is indium tin oxide (ITO) [9]. However, due to the relative scarcity, high cost and toxic effect of indium oxide, an extensive amount of research effort has been made to find alternative TCO materials [10]. Aluminum doped zinc oxide (AZO) is one of the potential candidates to replace ITO owing to its high electro-optical quality, abundance of materials, and non-toxicity. AZO exhibits similar optical and electrical properties to ITO, with AZO's optical transparency of >80% and small resistivity (large conductivity) values on the order of 10^{-4} $\Omega\cdot cm$ [9a, 11]. AZO thin films are proven to be beneficial for boosting nonlinear optical effects [6c, 12] and for developing tailorable nano-photonic devices [7d]. However, many of these studies show that the enhanced absorption and field intensity related to ENZ modes in AZO films are strongly dependent on the material properties as well as film thickness [13] . Hence, it is crucial to have precise control over both material properties and thickness in the fabrication process.

The pulsed laser-assisted deposition technique has been used in the past to synthesize AZO films with ENZ properties [4a, 7c]. However, this technique lacks thickness control on the order of one atomic layer (a few angstroms). In contrast, atomic layer deposition (ALD) is capable of synthesizing materials with thicknesses of just one atomic layer. ALD incorporates self-saturated and self-limiting chemical reaction processes [14] that enable sub-nanometer precision in thickness along with its unique ability to conformally coat high aspect ratio structures and pinhole free deposition [15]. Earlier works on ALD-based AZO thin films were focused on the

structural, morphological, and electrical properties of AZO films across the entire composition spectrum. The study of the optical properties of thin AZO films was limited to the optimization of their transmission and figure of merit. The latter is defined as the ratio of the electrical conductivity to the optical absorption coefficient of the film [16]. However, there has been no experimental study on ALD optimization of ENZ properties of ultra-thin (< 100 nm) AZO films with the ultimate motivation of engineering absorption and electric-field intensity enhancement (FIE) due to ENZ mode excitation in TCO thin films.

In this paper, we present methods to design absorption and FIE associated with ENZ modes in AZO nanolayers via control over the ENZ wavelengths, and optical losses (ε''), which can be changed by varying the ALD parameters such as dopant ratio, and deposition temperature. In addition, the ENZ properties of the ALD AZO nanolayers are strongly thickness dependent. Hence, film thickness, which is directly related to the number of macro-cycles in the ALD process, can be used as another control parameter to achieve the desired ENZ mode properties. Also, the ENZ wavelengths are tailorable in the near infrared region. We demonstrate ENZ mode excitation in these AZO nanolayers in the classical Kretschmann-Raether configuration and measure their absorption. Furthermore, we show how maximum absorption and FIE can be attained by changes to the ALD control parameters.

We believe that this detailed study on how to tailor absorption and FIE associated with ENZ modes in TCO films will be crucial for the design of next-generation energy-efficient optoelectronic, nonlinear, and quantum optical devices based on zero-index materials.

2. Results and discussion

2.1. Nano-engineering of ENZ wavelength (λ_{ENZ}) and loss of AZO thin film by varying ALD conditions

It is known that material and optical properties of ultra-thin ENZ films are strongly dependent on ALD parameters such as deposition temperature, dopant ratio, and thickness [17]. For ALD-fabricated AZO, we define the dopant ratio (X:1) as the number of monolayers (X) of ZnO to one monolayer of Al_2O_3 [13a]. A complete cycle of X monolayers of ZnO and one monolayer of Al_2O_3 is defined as a macro cycle. The thickness of the AZO nanolayers can be controlled by depositing for a desired number of macro cycles. Diethylzinc (DEZ) and distilled (DI) water were used as precursors to deposit a monolayer of ZnO film, and trimethylaluminium (TMA) and DI water were alternately introduced into the chamber for Al-doping of the ZnO films (see Figure 1). To study the impact of changing the ALD parameters on the ENZ properties of the AZO nanolayers, three sets of samples were deposited with different deposition temperatures, dopant ratios, and thicknesses (see *Experimental section* for fabrication details). The optical properties of the fabricated AZO nanolayers grown at different ALD parameters are characterized by spectroscopic ellipsometry measurements, and the results are shown in Figure 2.

2.1.1 Control by deposition temperature.

To study the ENZ wavelength and loss dependence on the deposition temperature, AZO nanolayers were deposited on silicon and silica substrates with dopant ratio 25:1, similar thickness, and different deposition temperatures ranging from 225°C to 275°C (see Table S1 in

Supporting Information). The optical properties of the fabricated AZO films grown at the different temperatures are shown in Figure 2a. The screened plasma frequency (ω_{sp}), collision frequency (γ), and ENZ wavelength $\lambda_{ENZ} = \frac{2\pi C}{\sqrt{\varepsilon_\infty \omega_{Sp}^2 - \gamma^2}}$, are plotted in Figure 2d-i. It should be noted that the relationship for ENZ wavelength given above is valid only in a case of AZO optical properties being described by the Drude model (see *Supporting Information* S1). The ENZ wavelength for the AZO nanolayers on silica and silicon substrates are comparable, because the optical properties of the nanolayers and their growth rates at different temperatures are similar for both substrates. (see *Supporting Information,* Figure S2 for temperature dependent growth rates and Table S1 for details of ellipsometry modelling).

It is clear from Figure 2d that the ENZ wavelength shifts to a shorter wavelength as the deposition temperature increases from 225ºC to 250ºC. The blueshift of the ENZ wavelength is attributed to the increase of doping efficiency (i.e. the ratio of electrically-active vs. incorporated Al) and the change in material crystal structure with the deposition temperature, as samples deposited with higher temperatures typically have more pronounced crystallinity and larger grain size [18]. This increase in electrically active Al-dopant with the increase in temperature is ascertained by the increase in screen plasma frequency and the decrease in collision frequency at 250ºC. The higher film crystallinity and larger grains lead to the reduction of scattering centers for free carriers, resulting in a lower collision frequency, which manifests as an increase in electron mobility [18a, 19]. Thus, the ENZ wavelength has a minimum value at 250ºC. However, for higher growth temperature (>250ºC), the ENZ wavelength shifted to a longer wavelength because of the increase in collision frequency (see Figure 2d). This increase in collision frequency can be associated with the desorption of precursors at the high temperatures during the deposition process which occurs because of the decrease of crystal quality and increase of internal defects [20]. It should be noted that there must be an optimum distance between neighboring Al^{3+} dopants to fully activate the extrinsic doping of ALD-AZO [21]. Any attempt to increase carrier concentration by incorporating more Al^{3+} dopants leads to clustering of these dopants which lead to carrier localization and reduced mobility. Thus the optimization of the distance between neighboring Al^{3+} dopants is governed by the deposition temperature as well as the dopant ratio [22]. Furthermore, the higher deposition temperatures also led to partial self-decomposition of DEZ molecules before the molecules reach the substrates (self-decomposition temperatures for DEZ and TMA are ~250ºC and 332ºC respectively). The self-decomposition of materials leads to reduced Al atoms substitution into Zn sites and introduces impurities in the thin film, thus increasing the scattering centers and decreasing the carrier concentration and electron mobility. Nevertheless, the ENZ wavelength could be tuned by the ALD temperature between ~1550 nm and 1700 nm.

2.1.2. Control by dopant ratio

We further investigated the effect of the dopant ratio on the ENZ properties of AZO nanolayers by growing AZO with varying dopant ratio (ZnO:Al) on silicon and silica substrates at a constant temperature of 250°C (Figure 2b). To negate the effect of thickness on optical and electrical properties, all thin films were grown with similar film thickness of 70 nm on silicon substrates (see Table S2 in *Supporting Information*). The ENZ wavelength dependence on dopant ratio is depicted in Figure 2e. Note that the decrease in dopant ratio (ZnO:Al) indicates

more layers of Al dopant in the AZO thin films (i.e., increase in Al dopant), resulting in high n-doping of ZnO by Al^{3+} ions [23]. When a Zn^{+2} ion in the ZnO lattice is replaced by an Al^{+3} ion, the Al^{+3} contributes an extra valence electron as a charge carrier. This increase in carrier concentration blue shifts the ENZ wavelength of the AZO thin film for the dopant ratio from 40:1 to 30:1. The increase in carrier concentration can be inferred from the increase in screen plasma frequency (see Figure 2e, h, k). At a dopant ratio 40:1 the number of charge carriers is reduced due to the lower Al concentration in the AZO nanolayers, resulting in red shifting of ENZ wavelength. However, there is an optimum thickness of ZnO between Al_2O_3 layers [22] to fully activate the extrinsic doping of ALD-AZO films which corresponds to the redshift of ENZ wavelength from the dopant ratio 30:1 to 20:1 (Figure 2e). Also, the decrease in collision frequency at this dopant ratio (30:1) suggest low clustering of Al-dopant, resulting in low incorporated Al-dopant.

2.1.3. Control by number of macro cycle (thin film thickness)

The role of AZO thickness in designing absorption and FIE associated with ENZ modes in AZO nanolayers is twofold. On the one hand, ultra-thin films are essential for sustaining the ENZ polariton modes and absorptance and FIE directly depend on the AZO thickness. On the other hand, the thickness of AZO nanolayers affects their ENZ properties and thus affects absorptance and FIE indirectly. Here, we show the effect of AZO nanolayer thickness on the ENZ frequency. To this end, AZO nanolayers with different numbers of macro-cycles were deposited at 250°C and a fixed 25:1 dopant ratio on silicon and silica substrates. The resulting AZO nanolayer thicknesses follow a linear dependence with the number of macrocycles (see *Supporting Information*, Figure S3a). Profilometer measurements were performed to confirm the AZO thicknesses obtained by ellipsometry and a good agreement between the two techniques was achieved (Figure S3a). Figure 2f shows the dependence between the ENZ wavelength of the AZO nanolayers and the number of macro-cycles of the deposition. We observed that the ENZ wavelength blue-shifts with an increase in the thickness and remained constant with further increase in thickness (> 25 macro cycles). This could be attributed to the fact that the Al doping sequence in ALD requires 1-3 nm of ZnO deposition in order to fully activate the doping substitution [14, 24], thus fewer free carriers are shown on thinner samples (resulting in longer ENZ wavelength) which is supported by a steady increase in the screen plasma frequency with thickness (Figure 2i). Thus, as the thickness increases, the ENZ wavelength blue-shifts and reaches a value that corresponds to a selected dopant ratio. Another possible contributing factor to the observed blue-shift is the increase in the grain size. AFM measurements show that the roughness of the AZO thin film increases from 2 nm to 5 nm with an increase of AZO thickness (The surface roughness of 2-5 nm is adequate for photonic applications in the visible and NIR regime) (see *Supporting Information*, Figure S3b). This increase in grain size lead to the blue-shift of the ENZ wavelength as discussed in 2.1.1. It should be noted that the parameter space for ENZ wavelength tuning has not been fully explored. Note that there is a preferential dissociation of TMA on silica substrate during the first stages of growth (Figure 2f), which leads to an increase of the collision frequency. However, the full understanding of early-stage AZO growth dynamics is outside of the scope of the present study. The ENZ wavelength of the film could be further altered by using a different set of deposition parameters and pulse durations of the deposition precursors. We showed in a separate experiment that the shorter

ENZ wavelength could be achieved with a dopant ratio of 30:1 and TMA pulse duration of 15 μs (see *Supporting Information*, Figure S4 for details). Thus, optimization of the pulse duration and other ALD parameters could provide further tunability on the ENZ properties.

2.2. Manipulate of optical absorption and field intensity enhancement of ENZ mode by ALD conditions.

Absorption and FIE depend strongly on optical losses at the ENZ frequency (ε''_{ENZ}) which, alongside with the ENZ frequency of AZO nanolayers, can be controlled by the ALD parameters. The ENZ losses of the three AZO series obtained via ellipsometry are shown in Figure 2g-i. Within the Drude model, there is a simple relationship between the ENZ losses, electron collision rate, and ENZ frequency: $\varepsilon''_{ENZ} = \frac{\varepsilon_\infty \, \gamma \, \lambda_{ENZ}}{2\pi c}$ (see *Supporting Information*, S1). It is clear that the loss is the lowest for the highest ENZ frequency and the smallest electron collision rate (for example the AZO nanolayers with 30:1 dopant ratio in Figure 2h). The losses increase whenever ENZ frequency decreases and/or collision/screen plasma frequency increases. The decrease in plasma frequency implies a decrease in the number of carriers. This implies a decrease in collision rate, which will reduce the optical losses, for example, the losses are larger in AZO nanolayers deposited at high temperature and with low dopant ratio. It is noteworthy that the losses are almost independent ($\varepsilon''_{ENZ} \sim 0.9$) of the thickness of AZO nanolayers (Figure 2i). Therefore, for a chosen dopant ratio and deposition temperature, the ENZ wavelength can be tuned by choosing a suitable thickness without a significant change in losses.

Here we discuss the effect of AZO nanolayer thickness and ENZ losses optimized by ALD parameters on enhanced absorption and FIE associated with ENZ modes. The enhanced absorption in the series of AZO nanolayers is revealed by measuring their specular reflectivity spectra in the Kretschmann–Raether configuration at a range of angles of incidence above the critical angle. Figure 3b shows ratios of TM and TE reflectivities measured from the AZO nanolayers of varying thickness at an angle of incidence of 42.3° along with the ratios calculated by the transfer matrix method (see *Experimental section* for details of the optical simulation). We observed a good agreement between measured and calculated reflectivities, which signifies the excitation of the ENZ polariton mode in AZO nanolayers. In the following we will be using the optical properties of AZO nanolayers obtained by ellipsometry for a more detailed assessment of the maximum absorptance and FIE. The perfect absorption is observed when the AZO film thickness satisfies the critical coupling condition [3b, 4a, 25]

$$\frac{2\pi t}{\lambda} = \frac{(\varepsilon')^2+(\varepsilon'')^2}{n_i^3\varepsilon''}\frac{1}{sin(\theta)\,tan(\theta)} \sim \frac{\varepsilon''}{n_i^3}\frac{1}{sin(\theta)\,tan(\theta)} \quad (|\varepsilon'| \ll \varepsilon''). \tag{1}$$

Here n_i is the refractive index of the incident medium, and θ is the angle of incidence. It must be noted that angle θ and wavelength λ in the Equation (1) are coupled by the dispersion relationship of the ENZ mode [3a, 25-26]. Equation (1) shows that the perfect absorption is achievable in ultra-thin ENZ film ($|\varepsilon'| \ll \varepsilon''$) if the optical losses ε'' are small. The optical losses of AZO nanolayers at ENZ wavelength are $\varepsilon''_{ENZ} \sim 0.9$ (Figure 2i), so that the perfect absorption is achieved in AZO nanolayers with the thickness $t > 78$ nm (or 30 macro-cycles). For example, at the angle of incidence of 42.3° (Figure 3a), we find the perfect absorption in

the AZO nanolayer with t ~ 152 nm (or 50 macro-cycles) at the wavelength of 1412 nm. It is noteworthy that at this wavelength $\varepsilon' \sim \varepsilon''$ and hence ε' in Equation (1) cannot be neglected. Figure 3b shows the TM-component of electric-field intensity distribution normal to the nanolayer surface calculated at the angle of incidence and wavelength of the maximum absorptance. Field intensity increases as the number of the deposition macro-cycles (nanolayer thickness) decreases. The maximum absorption and maximum FIE achievable in the AZO series due to the excitation of the ENZ mode are shown in Figure 3c. The perfect absorption is observed in thicker AZO nanolayers with the thickness t > 78 nm because of the optical losses associated with AZO.

The optical losses have a detrimental effect on FIE and its thickness dependence. FIE can be calculated from the absorptance using the following equation [41]:

$$FIE = \left|\frac{E}{E_i}\right|^2 = \frac{A(\theta,\lambda)\cdot n_i \cdot cos(\theta)}{\varepsilon''}\frac{\lambda}{2\pi t}. \quad (2)$$

Here E is the average field inside the AZO nanolayer, E_i is the incident field, and $A(\theta, \lambda)$ is the absorptance. Contrary to the published reports [3a, 27], FIE in real ENZ materials with optical losses increases more weakly than $1/t^2$ as the nanolayer thickness decreases [29]. Figure 3c shows that the maximum FIE achievable in the AZO nanolayers increases as the nanolayer thickness decreases. The moderate increase of FIE in comparison with the $1/t^2$ dependence (Figure 3c) is attributed to AZO losses at the ENZ wavelength, which slightly vary with the thickness (Figure 2f) and decrease in absorption (see Equation (2)). Note that FIE has its maximum at an angle of incidence and wavelength that are different from the angle and wavelength of the maximum absorptance as shown in the absorption and FIE contour plots in Figure 4. Therefore, the FIE optimization also differs from the absorptance optimization. For example, the thinnest AZO nanolayers are required for maximizing FIE, while on the contrary thick nanolayers are required for the perfect light absorption (Figure 3c and Figure 4). As the AZO thickness increases, the incidence angle of the maximum absorptance increases from 42.2° (the critical angle of ≈ 41.8°) to 45.5°, and the wavelength closely follows the ENZ wavelength (Figure 2f) until the thickness reaches about 78 nm (30 cycles) and the absorptance approaches unity. With further increase of the AZO thickness, the angle of incidence and wavelength of the perfect absorption decrease to 42.4° and 1412 nm, respectively, which can be attributed to a hybridization between the ENZ and surface plasmon-polariton modes. The maximum of FIE occurs around the critical angle regardless of the AZO nanolayer thickness, but its wavelength decreases from 1562 nm to 1311 nm when the AZO thickness increases (Figure 4). Equation 2 shows that FIE increases when the AZO losses decrease. Among the AZO nanolayers deposited at different temperatures and dopant ratios, smaller losses and hence larger FIE are observed in the nanolayers deposited at 250°C and the dopant ratio of 30:1 (see *Supporting Information*, Figure S5). AZO nanolayers with the shortest ENZ wavelength have smaller losses (see Equation S3) and therefore larger absorption and FIE.

We have shown that ENZ loss, ENZ wavelength, and AZO thickness can be controlled by ALD parameters to maximize absorptance and FIE of AZO nanolayers. It is important to note that optimization of ALD parameters of ultra-thin AZO ENZ films for zero-index applications is significantly different from maximizing a figure of merit (FoM) of conventional TCO materials, thus showing the significance of this study (see *Supporting Information*, Section S7 for the

details of FoM for conventional TCO materials).

3. Conclusions

We demonstrate a way to control FIE and absorption related to ENZ mode excitation in ALD-deposited AZO nanolayers via control over ALD parameters such as dopant ratio, deposition temperature, and number of macro-cycles. The deposited ENZ films are optically thin (thicknesses varying in between 20 nm and 160 nm) and their ENZ wavelengths lie in the near-infrared frequency region covering the optical communication bands (1500-1700 nm) and therefore suitable for small-footprint plasmonic applications. We also show that for lossy ENZ media (ZnO:Al nanolayers), FIE and absorption are highly dependent on film thicknesses, ENZ wavelengths (λ_{ENZ}) and imaginary parts of permittivity at ENZ wavelengths (ε''_{ENZ}) and we reveal the optimal FIE and absorption conditions. Our detailed systematic study on absorption and FIE associated with ENZ modes in TCO films will be helpful for the design and demonstration of energy-efficient optoelectronic, nonlinear, and quantum optical devices based on zero-index materials.

4. Methods

4.1. Atomic layer deposition of Al-doped zinc oxide thin film

AZO nanolayers were grown on silica and silicon substrates using an ALD reactor (Arradiance GEMSTAR-8TM Bench-Top system). The substrates were first cleaned by ultrasonication in acetone and isopropanol, rinsed with DI water, and dried with nitrogen gas [13a, 23, 28]. Diethylzinc (DEZ) and DI water were used as precursors to deposit ZnO films with pulse duration of 30 μs and 21 μs, respectively. High purity nitrogen gas was used for purging at 20 sccm for a purge period of 40 s between each pulse. For Al-doping of the ZnO films, trimethylaluminium (TMA) and H_2O were alternately introduced into the chamber with pulse duration of 30 μs and 21 μs to grow the Al_2O_3 layer. By repeating X monolayers of ZnO and then doping with 1 monolayer of Al_2O_3 resulted in AZO films with a high Al content [23]. The ratio of X cycles of DEZ-H_2O to one cycle of TMA-H_2O is known as dopant ratio (*X:1*), and this one complete process of X cycles DEZ-H_2O followed by one cycle TMA-H_2O is known as a macro cycle. The thickness of the AZO nanolayers was precisely controlled by repeating suitable numbers of the macro cycle [13a]. We prepared three set of samples where we changed the (1) deposition temperature, (2) dopant ratio, and (3) number of macro cycles (thickness). In the set for deposition temperature, only the deposition temperature was varied while keeping the dopant ratio (25:1) constant. In the dopant ratio series, deposition temperature was kept constant at 250°C and only the dopant ratio was varied with comparable thickness (see *Supporting Information*, Table S1 and S2). For the thickness series, we used the deposition temperature (250°C) and dopant ratio (25:1) and varied only the number of macro cycles.

4.2. Optical characterization

A spectroscopic ellipsometer (AngstromSun Technologies) with a spectral range from 400 to 1700 nm was used to measure the optical properties and the thickness of the AZO nanolayers at 55°, 60°, and 65°. The thickness of the AZO nanolayers was further confirmed using a profilometer. The surface roughness of the AZO nanolayers was measured using an atomic force microscope (Bruker). The ellipsometry measurement and fitting provided ε_∞, γ, and

ω_p along with the dispersion of the AZO thin films (see Table S1, Table S2, and Table S3). The dependence of the ENZ wavelength, screen plasma and collision frequencies on the ALD parameters is shown in Figure 2a-f. A typical ellipsometry data fitting is shown in Figure S1. (See *Supporting Information*, Sessions S1 and S2 and for details on the optical model).

4.3. Absorption measurement

The ENZ mode in AZO nanolayers is excited in the Kretschmann–Raether configuration [4a, 13a, 25]. Linearly polarized and collimated light from a supercontinuum laser source (broadband wavelength range of 600-1700 nm) is incident to the AZO nanolayer through a BK7 coupling prism (inset of Figure 3a). The coupling prism is affixed to a 0.5-mm-thick silica substrate of AZO nanolayer by means of a custom-made test fixture and BK7 index matching fluid. The specimen test fixture is mounted on a motorized rotary stage with a rotation angle of θ. The reflected light from the AZO nanolayer is collected by a multi-mode fiber fixed on another rotary stage with a rotation angle of 2θ. For both TE- and TM-polarization state of the incident light, the reflected light is recorded by an optical spectrum analyzer. The setup allows spectral reflectivity measurements over a broad angular range with an angular accuracy of 0.01°.

4.4. Simulation details

The absorptance of the AZO nanolayers and the electric-field intensities inside the films for different film thicknesses are calculated using the transfer and scattering matrix based tools [29]. TM polarized plane wave incidence was assumed and complex refractive indices of AZO nanolayers obtained by spectroscopic ellipsometry are used in the numerical simulations. Contour plots for normalized absorption and FIE are generated as functions of both the excitation wavelength and the angle of incidence. Results produced with the two different approaches (transfer matrix and scattering matrix) are in good agreement.

Associated Content

Supporting information. Drude model; Ellipsometric parameters of AZO nanolayers from the three deposition series: temperature, dopant ratio, and thickness; An example of ellipsometry data fit; Growth rate dependence of AZO nanolayers prepared on silicon and silica substrate at different deposition temperatures; Thickness and roughness measurements of various AZO nanolayers (thickness series); Thickness dependence of ENZ wavelength in AZO nanolayers deposited with reduced TMA pulse; ENZ properties of AZO nanolayers of varying dopant ratio (dopant series) and deposition temperature (temperature series); A TCO figure of merit (FoM) of AZO nanolayers of varying thickness (thickness series).

Notes

The authors declare no competing financial interests.

Acknowledgements

The authors acknowledge the support from the Young Faculty Award Program from the Defense Advanced Research Projects Agency (grant number N66001-17-1-4047), the CAREER Award Program from National Science Foundation (grant number: 1752295), the Robert A. Welch Foundation (Award number: AA-1956-20180324), the University Research Committee Grant Program from the Office of Vice Provost for Research at Baylor University, and the US Naval Research Laboratory Base Program. The authors acknowledge the Center for

Microscopy and Imaging (CMI) at Baylor University for technical support during the microscopy and image analysis.

References

[1] a) X. Niu, X. Hu, S. Chu, Q. Gong, *Advanced Optical Materials* **2018**, 6, 1701292; b) I. Liberal, N. Engheta, *Nature Photonics* **2017**, 11, 149.

[2] a) M. Z. Alam, I. De Leon, R. W. Boyd, *Science* **2016**, 352, 795; b) M. Silveirinha, N. Engheta, *Physical review letters* **2006**, 97, 157403.

[3] a) S. Campione, I. Brener, F. Marquier, *Physical Review B* **2015**, 91, 121408; b) S. Vassant, J.-P. Hugonin, F. Marquier, J.-J. Greffet, *Optics express* **2012**, 20, 23971.

[4] a) A. Anopchenko, L. Tao, C. Arndt, H. W. H. Lee, *ACS Photonics* **2018**; b) T. S. Luk, S. Campione, I. Kim, S. Feng, Y. C. Jun, S. Liu, J. B. Wright, I. Brener, P. B. Catrysse, S. Fan, *Physical Review B* **2014**, 90, 085411.

[5] a) R. Sokhoyan, H. A. Atwater, *Optics express* **2013**, 21, 32279; b) R. Fleury, A. Alu, *Physical Review B* **2013**, 87, 201101; c) L. Li, W. Wang, T. S. Luk, X. Yang, J. Gao, *ACS Photonics* **2017**, 4, 501.

[6] a) M. Z. Alam, I. De Leon, R. W. Boyd, *Science* **2016**, aae0330; b) O. Reshef, E. Giese, M. Z. Alam, I. De Leon, J. Upham, R. W. Boyd, *Optics letters* **2017**, 42, 3225; c) L. Caspani, R. Kaipurath, M. Clerici, M. Ferrera, T. Roger, J. Kim, N. Kinsey, M. Pietrzyk, A. Di Falco, V. M. Shalaev, *Physical review letters* **2016**, 116, 233901; d) A. Alu, M. G. Silveirinha, A. Salandrino, N. Engheta, *Physical review B* **2007**, 75, 155410; e) T. S. Luk, D. De Ceglia, S. Liu, G. A. Keeler, R. P. Prasankumar, M. A. Vincenti, M. Scalora, M. B. Sinclair, S. Campione, *Applied Physics Letters* **2015**, 106, 151103; f) A. Capretti, Y. Wang, N. Engheta, L. Dal Negro, *Optics Letters* **2015**, 40, 1500.

[7] a) C. Chen, Z. Wang, K. Wu, H. Ye, *Science and Technology of advanced MaTerialS* **2018**, 19, 174; b) G. V. Naik, V. M. Shalaev, A. Boltasseva, *Advanced Materials* **2013**, 25, 3258; c) G. V. Naik, J. Kim, A. Boltasseva, *Optical Materials Express* **2011**, 1, 1090; d) N. Kinsey, C. DeVault, J. Kim, M. Ferrera, V. Shalaev, A. Boltasseva, *Optica* **2015**, 2, 616.

[8] J. D. Caldwell, L. Lindsay, V. Giannini, I. Vurgaftman, T. L. Reinecke, S. A. Maier, O. J. Glembocki, *Nanophotonics* **2015**, 4, 44.

[9] a) H. Kim, a. C. Gilmore, A. Pique, J. Horwitz, H. Mattoussi, H. Murata, Z. Kafafi, D. Chrisey, *Journal of Applied Physics* **1999**, 86, 6451; b) T. Minami, *Thin Solid Films* **2008**, 516, 5822; c) O. Mryasov, A. Freeman, *Physical Review B* **2001**, 64, 233111.

[10] a) T. Minami, *Thin Solid Films* **2008**, 516, 1314; b) J. Cui, A. Wang, N. L. Edleman, J. Ni, P. Lee, N. R. Armstrong, T. J. Marks, *Advanced materials* **2001**, 13, 1476.

[11] a) G. Luka, T. Krajewski, B. Witkowski, G. Wisz, I. Virt, E. Guziewicz, M. Godlewski, *Journal of Materials Science: Materials in Electronics* **2011**, 22, 1810; b) P. Banerjee, W.-J. Lee, K.-R. Bae, S. B. Lee, G. W. Rubloff, *Journal of Applied Physics* **2010**, 108, 043504.

[12] a) G. P. Bharti, A. Khare, *Optical Materials Express* **2016**, 6, 2063; b) X. Tian, H. Luo, R. Wei, M. Liu, Z. Yang, Z. Luo, H. Zhu, J. Li, J. Qiu, *Nanoscale* **2019**, 11, 13988.

[13] a) A. Anopchenko, S. Gurung, L. Tao, C. Arndt, H. W. H. Lee, *Materials Research Express* **2018**, 5, 014012; b) H. Zheng, R.-J. Zhang, D.-H. Li, X. Chen, S.-Y. Wang, Y.-X. Zheng, M.-J. Li, Z.-G. Hu, N. Dai, L.-Y. Chen, *Nanoscale research letters* **2018**, 13, 149.

[14] J.-S. Na, Q. Peng, G. Scarel, G. N. Parsons, *Chemistry of materials* **2009**, 21, 5585.

[15] M. Ritala, M. Leskelä, J. P. Dekker, C. Mutsaers, P. J. Soininen, J. Skarp, *Chemical Vapor Deposition* **1999**, 5, 7.

[16] D. S. Ginley, C. Bright, *MRS bulletin* **2000**, 25, 15.

[17] V. Miikkulainen, M. Leskelä, M. Ritala, R. L. Puurunen, *Journal of Applied Physics* **2013**, 113, 2.

[18] a) E. Shkondin, O. Takayama, M. A. Panah, P. Liu, P. V. Larsen, M. D. Mar, F. Jensen, A. Lavrinenko, *Optical Materials Express* **2017**, 7, 1606; b) Z. Baji, Z. Lábadi, Z. E. Horváth, M. Fried, B. Szentpáli, I. Bársony, *Journal of thermal analysis and calorimetry* **2011**, 105, 93.
[19] Q. Hou, F. Meng, J. Sun, *Nanoscale research letters* **2013**, 8, 144.
[20] J. Guan, Q. Duanmu, presented at 2017 IEEE International Conference on Manipulation, Manufacturing and Measurement on the Nanoscale (3M-NANO) **2017**.
[21] K. Ellmer, A. Bikowski, *Journal of Physics D: Applied Physics* **2016**, 49, 413002.
[22] D. J. Lee, H. M. Kim, J. Y. Kwon, H. Choi, S. H. Kim, K. B. Kim, *Advanced Functional Materials* **2011**, 21, 448.
[23] J. Elam, D. Routkevitch, S. George, *Journal of the Electrochemical Society* **2003**, 150, G339.
[24] J.-S. Na, G. Scarel, G. N. Parsons, *The Journal of Physical Chemistry C* **2009**, 114, 383.
[25] S. Campione, I. Kim, D. de Ceglia, G. A. Keeler, T. S. Luk, *Optics express* **2016**, 24, 18782.
[26] S. Campione, D. de Ceglia, M. A. Vincenti, M. Scalora, F. Capolino, *Physical Review B* **2013**, 87, 035120.
[27] a) M. Kamandi, C. Guclu, T. S. Luk, G. T. Wang, F. Capolino, *Physical Review B* **2017**, 95, 161105; b) J. Yoon, M. Zhou, M. A. Badsha, T. Y. Kim, Y. C. Jun, C. K. Hwangbo, *Scientific reports* **2015**, 5, 12788.
[28] H. Saarenpää, T. Niemi, A. Tukiainen, H. Lemmetyinen, N. Tkachenko, *Solar Energy Materials and Solar Cells* **2010**, 94, 1379.
[29] a) N. Cotter, T. Preist, J. Sambles, *JOSA A* **1995**, 12, 1097; b) C. C. Katsidis, D. I. Siapkas, *Applied optics* **2002**, 41, 3978.
[30] A. Anopchenko, S. Gurung, S. Bej, and H. W. Lee, submitted in Physical Review Letters.

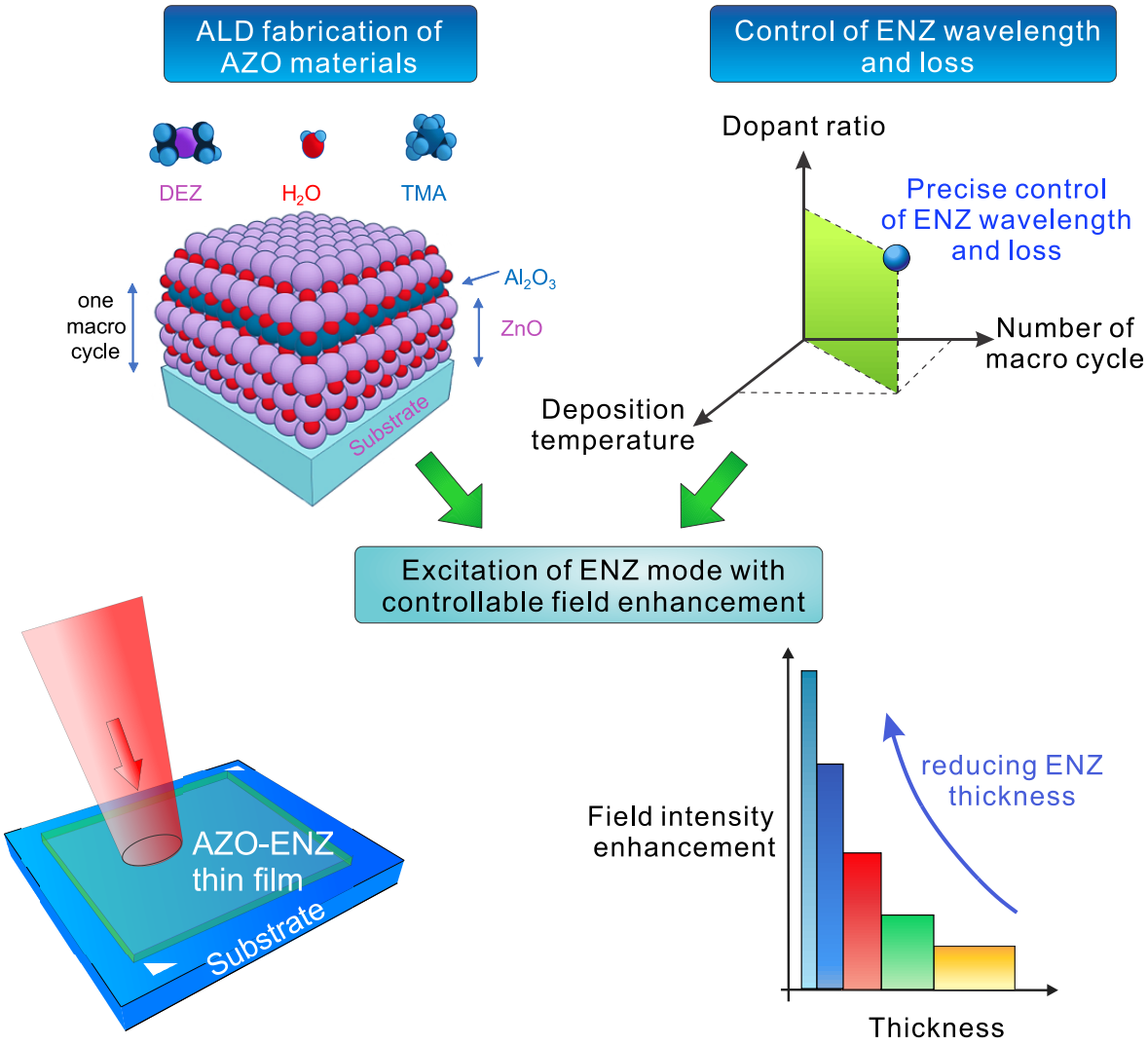

Figure 1. Schematic of atomic layer deposition process of Al-doped zinc-oxide ENZ materials. ENZ wavelength, loss, and thickness of the AZO thin film are precisely controlled by appropriate selection of dopant ratio, deposition temperature and number of macrocycles during the deposition process. X-monolayers of ZnO are deposited and doped with 1-monolayer of Al_2O_3, and the ratio X:1 is defined as dopant ratio and X+1 cycle as one macrocycle. The excitation of the ENZ mode and the field intensity enhancement within the AZO-ENZ thin films are controlled by the loss and thickness of the AZO nanolayers.

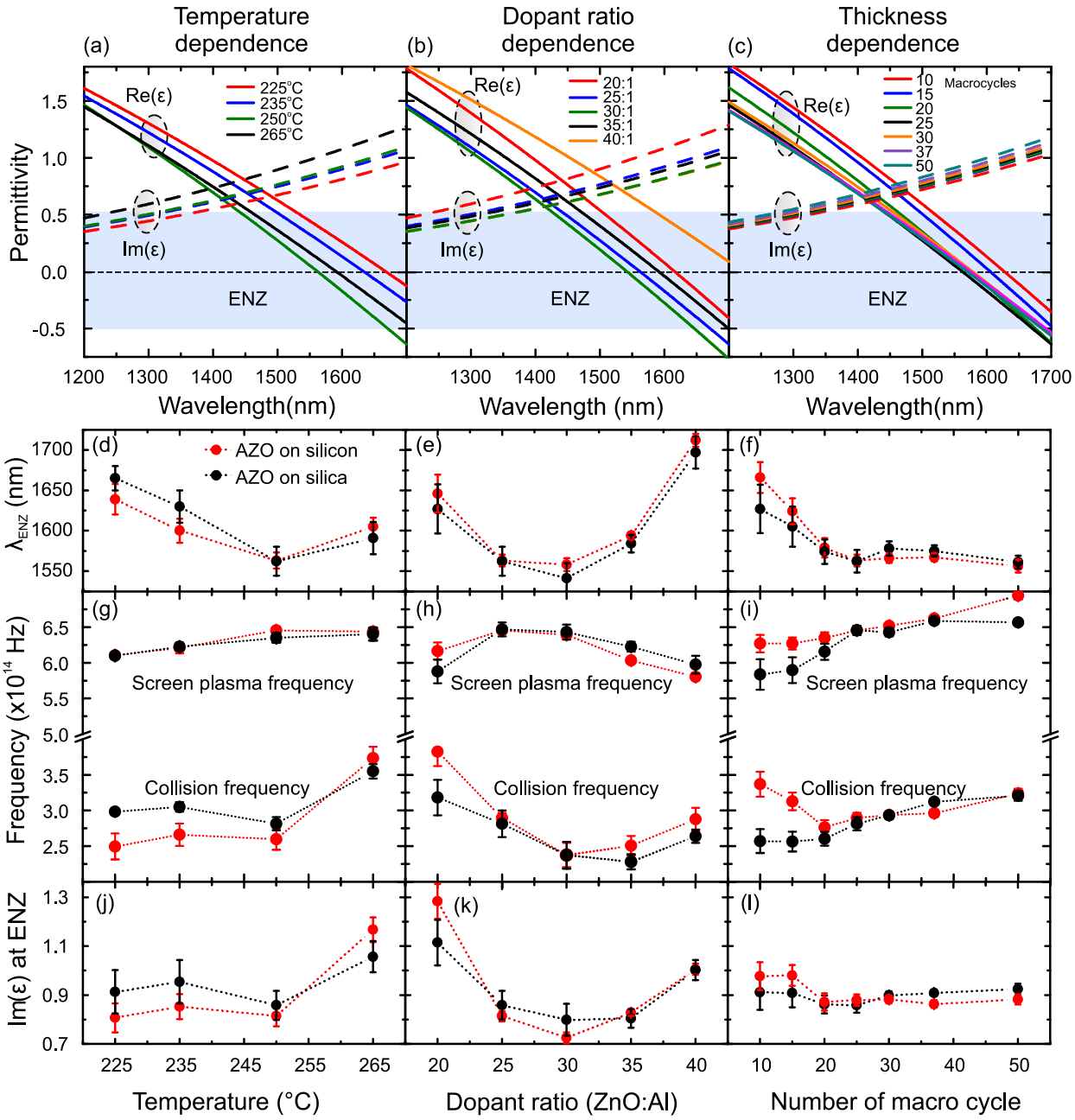

Figure 2. (a-c) Wavelength dependence of the real (ε') and imaginary (ε'') part of permittivity of AZO nanolayers obtained by ellipsometry measurements. AZO nanolayers were prepared on silica substrates with different ALD parameters: deposition temperature, dopant ratio, and number of macro cycles (thickness). The red and black circles represent data points with AZO on silicon and silica, respectively. Dependence of (d-f) the ENZ wavelength, (g-i) the Screen plasma and collision frequencies, and (j-l) the imaginary part of permittivity at ENZ wavelength (ε''_{ENZ}) on different ALD parameters. (d, g, j) For the temperature dependence, AZO nanolayers were prepared at different deposition temperatures at 25:1 dopant ratio (see Table S1). (e, h, k) For the dopant ratio dependence, AZO nanolayers were prepared for different dopant ratio at 250°C (see Table S2). (f, i, l) For the number of macro cycles dependence, AZO nanolayers were prepared with different thicknesses for dopant ratio 25:1 and deposition temperature 250°C (see Table S3).

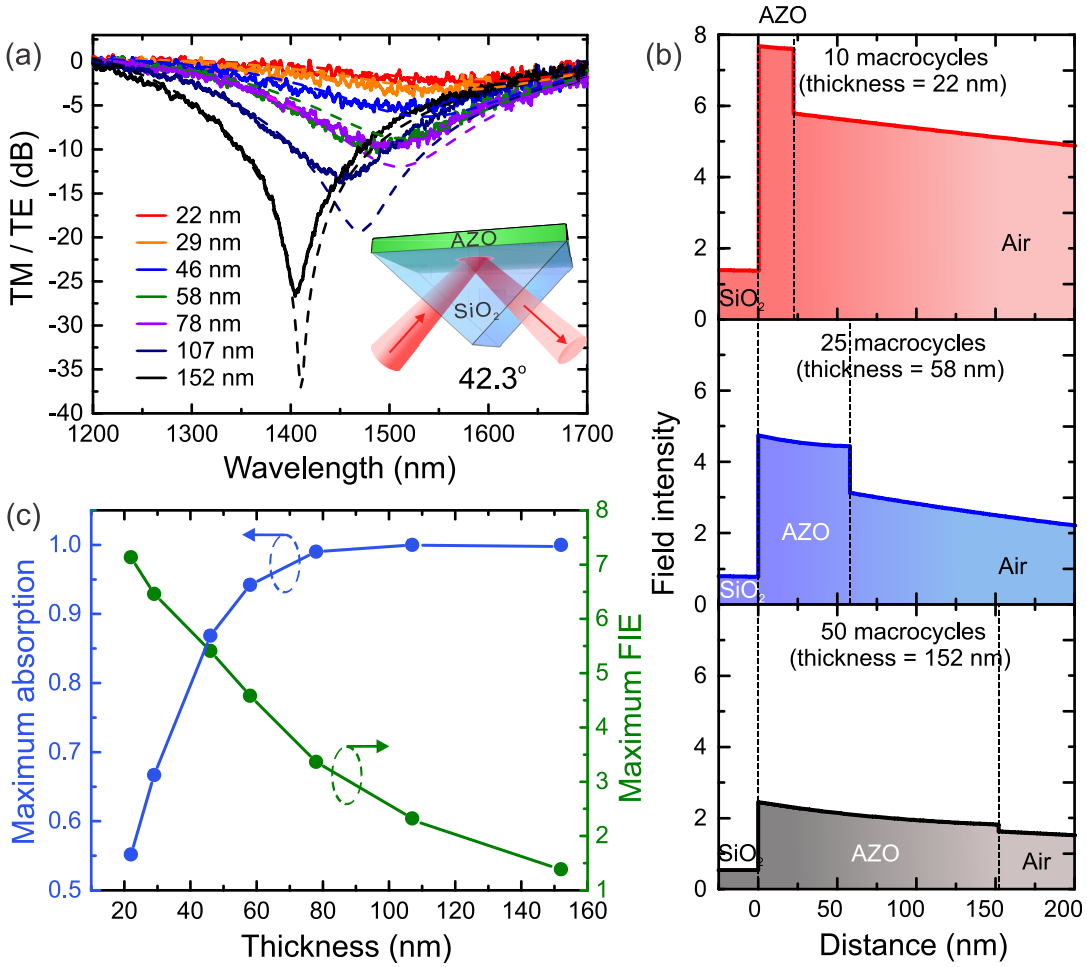

Figure 3(a) Measured (solid curves) and simulated (dashed curves) ratios of the TM- and TE-polarized reflectivities in the Kretschmann–Raether configuration at a fixed angle of incidence of 42.3° (inset) for different thicknesses of the AZO nanolayer fabricated on silica substrate with 25:1 dopant ratio and 250°C deposition temperature. The reflection dip is resulted from the excitation of the ENZ polariton mode on AZO layer. (b) Simulated field intensity distributions with AZO nanolayers for different thicknesses using the measured dispersion of the AZO. (c) Maximum absorption and maximum field intensity enhancement dependence on the thickness of AZO nanolayers. Maximum absorptance is calculated using the transfer matrix method and FIE was calculated from Equation (2) based on the experimentally measured optical constants. Note that the angle of incidence and wavelength for maximum absorption and FIE are different (see Figure 4).

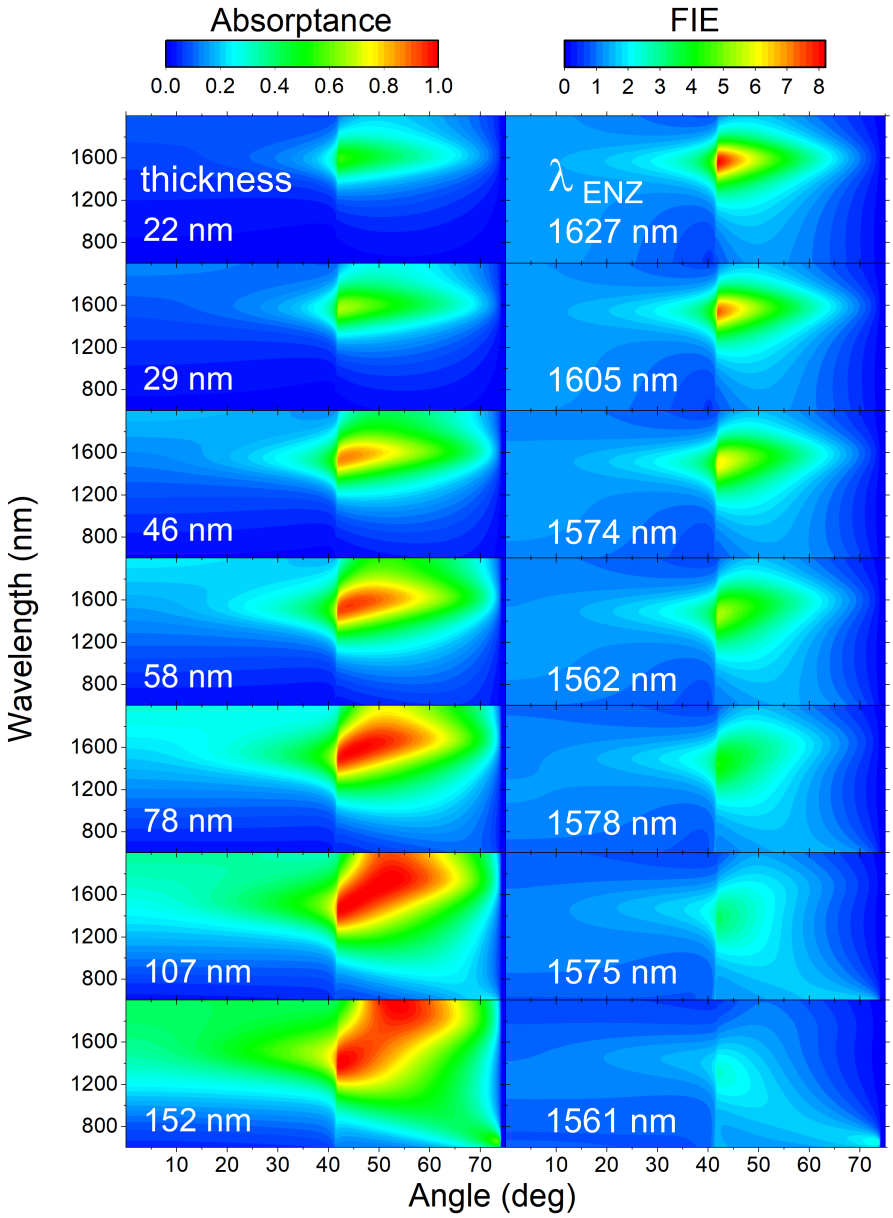

Figure 4. (Left column) Absorptance in the Kretschmann–Raether configuration calculated using the transfer matrix method for AZO nanolayers of different thicknesses (the thickness series) deposited on silica substrates. Plane wave incident from a BK7 prism attached to the substrate. The critical angle of ≈ 41.8° is observed in the figure. (Right column) Corresponding FIE calculated from Equation (2) using the absorptance data on the left. For the thicker films (>100 nm), we observed high absorption at larger wavelengths which can be attributed to the hybridization between the ENZ and surface plasmon-polariton modes